Journal of Fluids and Structures (1994) **8**, 637–660

PREDICTION AND MEASUREMENT OF THE AREA–DISTANCE PROFILE OF COLLAPSED TUBES DURING SELF-EXCITED OSCILLATION

C. D. BERTRAM AND M. D. SHEPPEARD
Centre for Biomedical Engineering, University of New South Wales
Sydney, Australia 2052

AND

O. E. JENSEN
Department of Mathematics & Statistics, University of Newcastle upon Tyne
Newcastle upon Tyne NE1 7RU, U.K.

(Received 16 April 1993 and in revised form 27 January 1994)

The internal cross-sectional area of collapsible tubes undergoing self-excited oscillation is investigated as a function of both time and streamwise position. Numerical predictions are made using a nonlinear one-dimensional model which incorporates longitudinal wall-tension effects and dissipation due to flow separation. Experimental measurements are made with a conductimetric catheter at successively incremented axial locations, using the sharply defined minimum of the pressure waveform at the downstream end of the tube to provide a phase reference. This methodology is limited to strictly periodic oscillations. The waveform chosen for both simulation and observation was of low frequency, with a prolonged collapse phase. Despite unavoidable parameter differences between theory and experiment, the qualitative similarity between the predicted and empirical results suggests that the model captures many essential features of this mode of collapsible-tube oscillation. The model has also been previously shown to predict the observed change to a mode of some two to three times the frequency as the pressure outside the tube is increased; the present observations support the prediction that the two modes share a common mechanism.

1. INTRODUCTION

THE SIMULTANEOUS APPLICATION TO FLEXIBLE TUBES of a through-flow at substantial Reynolds numbers and of an external pressure causing the cross-section to flatten leads readily to the production of sustained oscillations. These oscillations present particular difficulties to both theoretician and empiricist. Theoretical models must encompass both the strong nonlinearity of the relationship between local transmural pressure and local cross-sectional area, and the high degree of coupling between the fluid flow and the boundary configuration. Measurements must avoid interfering with the vigorous motion of the tube wall and, equally, leave unperturbed the flow patterns within.

A degree of similarity is evident in the responses of mathematicians and experimentalists to these challenges. The theoretical lumped-parameter model (Conrad 1969; Schoendorfer & Shapiro 1977; Cancelli & Chiocchia 1979; Bertram & Pedley 1982) specifies the time-varying quantities at only a few important sites along the tube, and thereby secures the advantage of working with ordinary differential equations. Such models can incorporate effects arising at regions of rapid change of shape or cross-section, for example flow separation, but no description of wave travel is possible. A parallel scheme of experimental approach has involved the measurement of

0889–9746/94/060637 + 24 $08.00

time-variables at chosen fixed sites, usually at the tube extremities [e.g., Conrad (1969); Bonis (1979); Lyon *et al.* (1981); Ohba *et al.* (1984)]. This has sometimes been extended to the measurement of a specific time-variable within the tube, using either a catheter (Bertram 1986) or through-the-wall technique (Mazghi 1986) or an otherwise prepared tube (Bertram & Ribreau 1989). By common consent, the utility of further such investigations is waning. Theoretical progress now rests largely with the hybrid models which combine lumped elements in regions of rapid change with continuous spatial evolution of time-variables elsewhere (Cancelli & Pedley 1985; Jensen & Pedley 1989; Matsuzaki & Matsumoto 1989). For a full test, such models demand experimental data on one or more of the critical variables in equivalent distributed form. No ideal way of providing these data currently exists. Multi-sensor catheter techniques are not feasible for the number of distinct locations required. Perhaps the closest to the ideal is the measurement of cross-sectional area from oblique images of lines projected or scribed on the outside wall (Rosenberg *et al.* 1990; Elad *et al.* 1992). One camera then yields data for as many locations as there are lines. In practice there are problems: the resolution is dubious, and assumption rather than measurement provides the parts of the perimeter not visible to the camera's line of sight. As currently realized, the system is also complex and expensive.

Provided that strictly repetitive oscillations are to be observed, a simpler alternative is to build up a picture of the desired variable by successively recording its time-waveform at progressively incremented locations. For a one-dimensional formulation, the three variables of interest are the tube cross-sectional area, $\alpha(x, t)$, the internal pressure, $p(x, t)$ and the flow-speed, $u(x, t)$, where x is the longitudinal coordinate and t time. It is assumed that the cross-stream variation of p and u is small enough for each to be represented by its cross-sectional average. While u does not therefore correspond to any experimentally measurable quantity, the product $\alpha u = Q$, the local volume flow-rate, *is* accessible experimentally. However, it is easier to measure the local area, with the impedance technique (McClurken 1978), or the local pressure. We have investigated the practicality of such incremental acquisition in the context of collapsible-tube oscillations (Bertram & Sheppeard 1991) using a conductimetric catheter and a conveyor belt, as described by Kececioglu *et al.* (1981) for the acquisition of *static* area-distance profiles. The results obtained by this technique are compared below with area-position profiles computed from the theoretical model used by Jensen (1992). The model predicts several other quantities in addition to those which are measured experimentally here.

The parameter dependence of the experimental results is best viewed in terms of what in nonlinear dynamics is called a control–space diagram. The axes are the two control variables used to set a required operating point. These are the upstream pressure, p_u, driving the flow, and the pressure external to the tube, p_e. The control–space diagram shows regions of oscillatory instability, at low frequency (2–4 Hz), intermediate frequency (8–12 Hz), and high frequency (from about 60 Hz upwards). These regions are quite distinct. However, as shown previously (Bertram *et al.* 1991), a modified control–space diagram is preferable for this system, utilizing instead of p_e the time-averaged negative transmural pressure at the downstream end of the tube, i.e. external pressure minus mean internal pressure at the downstream end, or $\bar{p}_{e2} = p_e - \bar{p}_2$. In this form the diagram also shows explicitly the regions of divergent instability (Bertram 1986; Bertram *et al.* 1990), where the dependent variables $\bar{A}$ (the time-averaged tube minimum area), $\bar{p}_1$ (the time-averaged pressure at the upstream end of the tube), $\bar{p}_2$, $\bar{Q}_1$ and $\bar{Q}_2$ (the time-averaged flow rates at each end of the tube) all change discontinuously as p_e is progressively adjusted.

Because of the jump in frequency between successive oscillatory regions found experimentally, and the large gap in frequency between the observed intermediate-frequency and high-frequency regions in particular (Bertram *et al.* 1990), we were initially inclined to regard these regions as being the result of different oscillation mechanisms. However, subsequently, calculation showed that regions with approximately these frequency ratios might be due to different modes of a single oscillation mechanism (Jensen 1990b), the spacing of the frequency bands being accounted for by the dispersive effect of longitudinal wall-tension. Jensen (1990b) also showed that for small-amplitude oscillations, at parameter values near the apppropriate boundaries of stability, each mode exhibited a different number of maxima along the tube in the amplitude of area fluctuations. More recent computations show that for larger-amplitude oscillations, such a mode-specific pattern of maxima persists, but is less distinct (see below). Thus an important test of the theory is to compare the theoretical and observed patterns of tube area versus distance along the tube and versus time, in the different regions or modes, and see whether the predicted patterns of maxima are observed. The results of this test form the main subject of this paper. The methods used to measure the area profiles are described in Section 2. The theoretical model is briefly summarized in Section 3. The observations are presented in Section 4. The corresponding theoretical predictions are described in Section 5. In Section 6, the measured and predicted area–distance profiles are examined further, in conjunction with numerical predictions of variables that could not be measured, to provide a detailed analysis of events during a cycle of oscillation. The overall success of the comparison is discussed in Section 7.

2. EXPERIMENTAL METHODS

In the impedance technique for measuring local cross-sectional area of a tube (McClurken 1978), an alternating electric current is arranged to flow between electrodes up- and downstream of the tube, through the ionically conducting liquid within. This creates an alternating electric field gradient which is measured as a small potential difference using a catheter with two closely spaced electrodes. For area–distance profiles, the catheter was made part of a conveyor belt arrangement, so that it could be kept taut and its position could be readily incremented, and then recorded electrically *via* a potentiometer linked to the belt motion. At each position a recording of time-varying area was made, then the belt was moved on a constant amount, pulling the catheter through the tube *via* leakproof glands. If the catheter lies on the axis of the tube, it interferes with the motion of the throat at the point of maximal collapse. Instead, it was positioned so that it lay in one side-lobe of the cross-section. In this position the system still registers the local cross-section of the whole tube (Bertram 1987).

The area-measurement system has been shown previously to give an output voltage which is linearly related to the area of the conduit (McClurken 1978; Bertram 1986). The linearity does not extend right to zero, because the electronic divider responsible for taking the reciprocal of the demodulated catheter-measured voltage difference has a limited dynamic range. By extrapolation of calibration tests it can be verified that the zero-voltage intercept corresponds to the cross-sectional area of the catheter itself (Bertram 1987). This was used as one point of calibration; the other was the cross-sectional area of the tube at zero transmural pressure, which by definition is $\alpha = 1$. Prior to measurement, the performance of the system was checked by measuring the area profile of a long cylindrical tube, because various phenomena can cause the

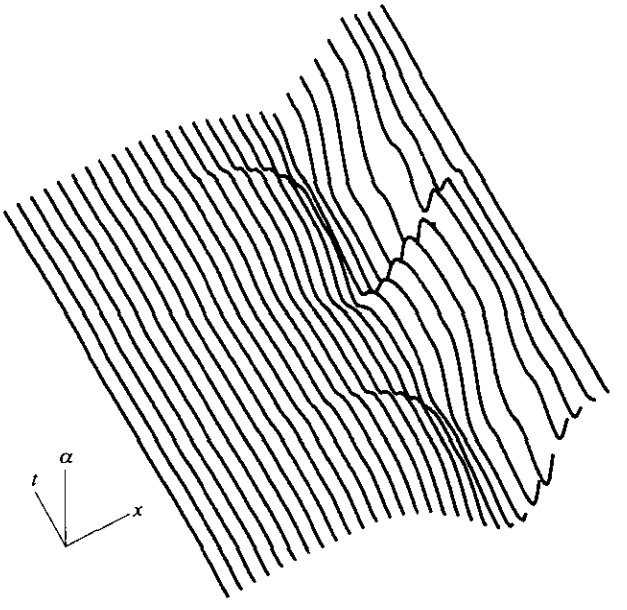

Figure 1. Area versus axial position and time for an LD oscillation, of frequency 4·3 Hz. Lines show area measurements made at 29 fixed positions. Parameter values: $p_u = 66$ and $\bar{p}_{e2} = 48{\cdot}1$ kPa, giving $\bar{Q} = 220$ ml/s. Time increases in the direction away from the viewer. The measurements shown cover the downstream 75 mm (32%) of the tube.

measured are to vary systematically from one end to the other. Countermeasures include maximizing the common-mode rejection performance of the processing electronics (Kececioglu *et al.* 1981). The calibration was checked with respect to the known area of the rigid pipe to which the flexible tube was joined at each end.

The α, x (axial position) and p_2 signals were digitized at 500 Hz using the greater part of the range of a 12-bit a.d.c. Subsequently the whole series of recordings at different positions were lined up and re-plotted as a three-dimensional graph of area versus distance and time; see for example Figure 1. For the lining-up, the sharply defined minimum of p_2 was used as a timing reference.

The accuracy of the technique was checked in two ways. First, since this methodology relies on the operating point giving stable oscillations which can be overlaid, we measured the extent of discrepancy between cycles recorded at the *same* position, due to either cycle-to-cycle variation or error in the lining-up procedure using p_2. An example of several overlaid cycles under these conditions is shown in Figure 2.

Second, the amount of additional error due to inaccurate catheter positioning was assessed by recording many cycles at one position but displacing and restoring the catheter position in between. From these tests it was calculated that the total combined error in α was of the order of $\pm 0{\cdot}02$ when $\partial\alpha/\partial t$ was small, amounting to 7% when α was small and less when it was large.

The operating point used for these experiments was from the region identified as LD by Bertram *et al.* (1991) on the control–space diagram for a tube approximately 17 diameters long and for a low value of downstream resistance [see Figure 2(g) of Bertram *et al.* (1991)]; further experimental parameters are given in Appendix A]. The LD notation denotes an oscillation of low frequency (about 4 Hz) with a relatively prolonged phase of tube collapse at the throat. This mode was chosen in preference to the other low-frequency mode (LU), in which the throat collapse is brief relative to the cycle period, because the LD mode resembled more closely the sinusoidal oscillations

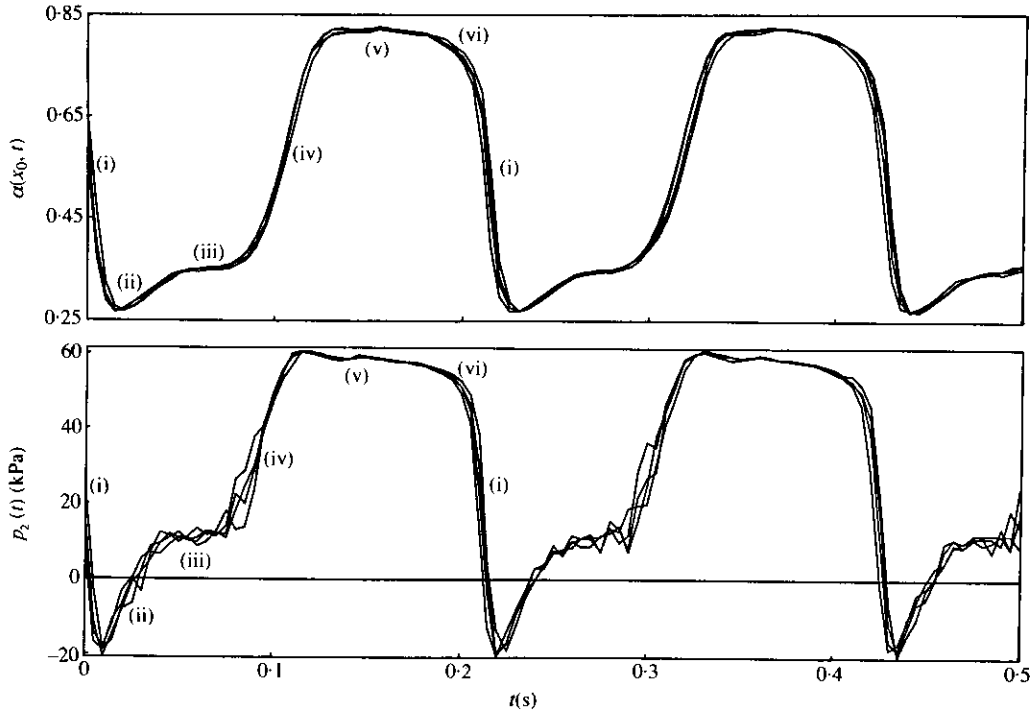

Figure 2. Errors due to lining up and to incompletely periodic oscillation. The waveforms shown are $\alpha(x_0, t)$ and $p_2(t)$ versus time t, where x_0 is the fixed position of the catheter electrodes, near the (slightly variable) point of minimum area. The oscillation is annotated in six phases, (i)–(vi), for comparison with Figure 9.

described by the linear stability theory used by Jensen (1990b). Recordings digitized at 200 Hz were also made at an I-region (intermediate-frequency) operating point.

3. THE THEORETICAL MODEL

The theoretical model is based upon four major assumptions: (i) the dominant source of dissipation is due to flow separation; (ii) the tube wall is thin enough to be treated as a thin membrane; (iii) the tube shape and the flow vary over long wavelengths, allowing a one-dimensional description of the problem; and (iv) the dominant forces in the tube wall are transverse bending (or stresses) and longitudinal tension.

The equations of the model, derived using these assumptions, have been given by Jensen (1990b, 1992), but for convenience are repeated here. The system is formed of fluid mass and axial-momentum conservation equations, which in nondimensional form are

$$\alpha_t + (\alpha u)_x = 0, \qquad u_t + \chi u u_x = -p_x$$

(subscripts in x and t denote partial derivatives), the latter modified by a factor χ to take account of the energy losses associated with flow separation beyond a constriction in the tube, and a pressure–area relationship

$$p - \hat{p}_e = \mathcal{P}(\alpha) - \tfrac{1}{2}\alpha_{xx} \qquad \text{with} \qquad \mathcal{P}(\alpha) = \begin{cases} 1 - \alpha^{-3/2} & \text{for } 0 < \alpha \leq 1 \\ k(\alpha - 1) & \text{for } \alpha > 1 \end{cases},$$

comprising a nonlinear 'tube law' $\mathcal{P}(\alpha)$ (in which k is a constant) representing

transverse stresses and bending in the tube wall, and a longitudinal tension term proportional to α_{xx}. The latter makes the system fourth-order in space, so the boundary conditions were that $\alpha = 1$ at each end of the tube and that the pressure at these points matches that determined by the apparatus up- and downstream, thereby taking into account the resistance and inertance of the rigid parts of the system (for details see Appendix A). This model is a development of that proposed by Cancelli & Pedley (1985), and shares many features, in particular the expression $d = (\chi - 1)uu_x$ for dissipation due to flow separation ($\chi = 1$, so that $d = 0$, where the flow was fully attached; $\chi = 0{\cdot}2$ arbitrarily, where the flow was separated). An important difference from that model concerns the location at which the flow leaving the tube throat is assumed to separate. Cancelli & Pedley (1985) and Matsuzaki & Matsumoto (1989) assumed that the flow separates at a point which depends hysteretically on the magnitude of the adverse pressure gradient. As in Jensen (1992), the separation point was here chosen to be where the flow speed was maximal (so that the dissipation d increased smoothly from zero across the separation point). In *steady* flow, this is also the point of minimum area and, in the absence of other dissipation mechanisms (Jensen & Pedley 1989), of minimum pressure. Contributions to the dissipation in the flow due to frictional forces are neglected in this model, being assumed negligible compared to the dissipation associated with flow separation.

In the theoretical model, the natural parameters governing steady flows are the values of Q and p_{e2} (Jensen & Pedley 1989). These same two quantities were used to parametrize *unsteady* solutions also, because for the values of other parameters assumed in the calculations, there existed unique steady (nondimensional) values of $\hat{p}_u$ and $\hat{p}_e$ for a given Q and p_{e2} (Jensen 1990b). (Note that in general the steady Q meant here is that in the absence of oscillation, and is not the same quantity as the time-averaged Q_2 during oscillation.)

The experimental and theoretical parameterizations are therefore equivalent. Complete matching of parameter values was not possible, however, for the following reason. The model is one-dimensional, and therefore rests centrally on assumption (iii) above that the tube shape varies slowly along the tube. The validity of this assumption requires $D_0 \ll L_0$, where D_0 is the internal diameter of the tube and L_0 [defined as $(D_0 T/K_p)^{1/2}$, where T is the longitudinal tension per unit perimeter and K_p the circumferential bending stiffness] is a length-scale of longitudinal variation over which forces due to longitudinal wall tension and transverse bending stiffness balance one another. This approximation is suited to thin-walled tubes, because they typically have small bending stiffnesses and thus large L_0/D_0. Under such conditions, and in steady flow, the model is quantitatively accurate (Jensen & Pedley 1989).

However, extremely thin-walled tubes joined to a rigid downstream pipe can undergo large-amplitude oscillations involving a phase of suction into the pipe. Such a motion is neither physiological nor within the scope of current theoretical modelling. Tubes of greater wall thickness, in which the longitudinal bending stiffness of the wall is a significant restoring force, are therefore preferable experimentally. A relatively thick-walled tube was used in the experiments described here, with $h/D_0 = 0{\cdot}15$, where h is the wall thickness; note that assumption (ii) requires $h/D_0 \ll 1$. For such a tube, K_p is necessarily large also, making L_0 small: in the present case $L_0 = 9{\cdot}4$ mm, less than one internal diameter ($D_0 = 13{\cdot}5$ mm). Terms in the model's governing equations that were neglected under assumption (iii) can therefore be expected to be of $O(1)$ magnitude, producing significant error. In addition, neglect of longitudinal bending stiffness may be significant: an argument presented in Appendix B, albeit based on assumptions (ii) and (iii), indicates that for the tube used in the experiments the effects

of longitudinal bending, longitudinal tension and transverse bending of the tube wall are all equally important. Quantitative comparison of the numerical predictions with the experimental results of Bertram (1986) and of Bertram *et al.* (1990, 1991), and with those described here, was not therefore achieved.

Nevertheless, qualitatively good agreement with the above series of experiments in respect of predicted steady flows and frequency ratios between low, intermediate and high frequency modes have been reported previously (Jensen & Pedley 1989; Jensen 1990b). An idea of the correspondence between p_u and Q as parameters may be gained by inspection of figure 12 in Bertram (1986), where constant-p_u curves and constant-$\bar{p}_{e2}$ curves are plotted in $(\bar{Q}_2, \bar{p}_{12})$-space. Since the patterns of stability boundaries in (experimental) $(p_u, \bar{p}_{e2})$-space also have clear similarities to those in (theoretical) (Q, p_{e2})-space (Jensen 1990b), the examples chosen for comparison below come from two regions sharing roughly identifiable locations; this is the extent to which parameters could be matched (full details of parameter values are given in Appendix A).

MacCormack's scheme (Roache 1976) was suitable for integration of the governing equations. This is an explicit, two-step method which is second-order accurate in both space and time. In the computations reported below, 101 grid points were distributed uniformly along the length of the tube. A detailed account of the application to this problem was given by Jensen (1990a).

Although the numerical method was successful in describing low-frequency oscillations of the LD type (see below), LU oscillations [e.g. figure 6(a) in Bertram *et al.* (1990)] could not be reproduced. This may be related to a fundamental difficulty in the model of flow separation, namely that at large amplitudes when variables are varying rapidly, the quasi-steadiness implicit in the choice of separation point (the point where $u_x = 0$) is unlikely to be accurate. The model predicted multiple regions of dissipation for very vigorous oscillations, for example, which is physically unreasonable. This difficulty was not encountered in the results described in the following.

4. EXPERIMENTAL RESULTS

From data as shown in Figure 1 can be extracted the maximum and minimum cross-sectional area reached during an oscillation at each catheter position, and from these in turn is derived a profile of peak-to-peak area-oscillation amplitude *versus* position. Figure 3 shows such a profile, for an experiment in which recordings were made right to the upstream end of the tube. The main peak defines the position of the throat unambiguously. The secondary peak does not correspond to theoretical prediction (a broad plateau extending from the upstream end—see Figure 11 here, or figure 6(a) in Jensen & Pedley 1989); it is much closer to the throat than was expected. However, this was a consistent finding. As shown in Figure 3, no other maximum of significance was found to occur upstream.

The two experiments shown in Figures 1 and 3 involved recordings every 2·9 mm and every 2·8 mm along the tube respectively. To verify further the existence of the secondary peak, an experiment was conducted with a position increment of only 1·15 mm, covering the downstream part of the tube as shown in Figure 4. Here, all points along the tube which have the same phasing, or time-delay after the fiducial point, have been joined; the result is more finitely delineated than would be the case with lines of $\alpha(t)|_x$, because of the high sampling rate. The result appears to show a smoother and more gradual amplitude maximum than that in Figure 3, because only the last downstream 15% of the tube is shown here. Note that the oscillation upstream

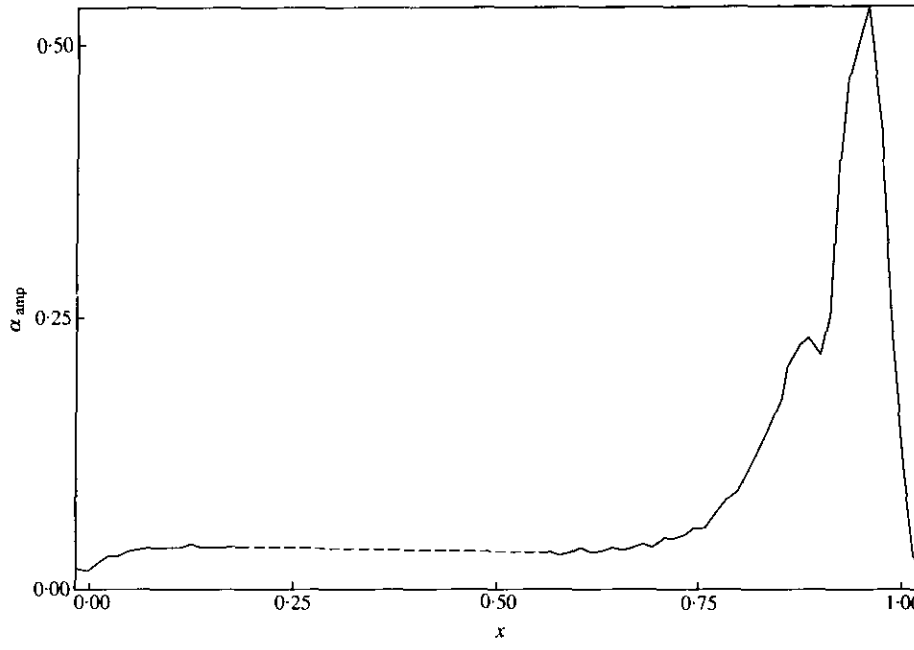

Figure 3. Area amplitude versus axial position, for an experiment in which recordings were made along the whole length of the tube. Parameter values: $p_u = 66$ and $\bar{p}_{e2} = 49{\cdot}7$ kPa. Frequency of oscillation: 4·5 Hz.

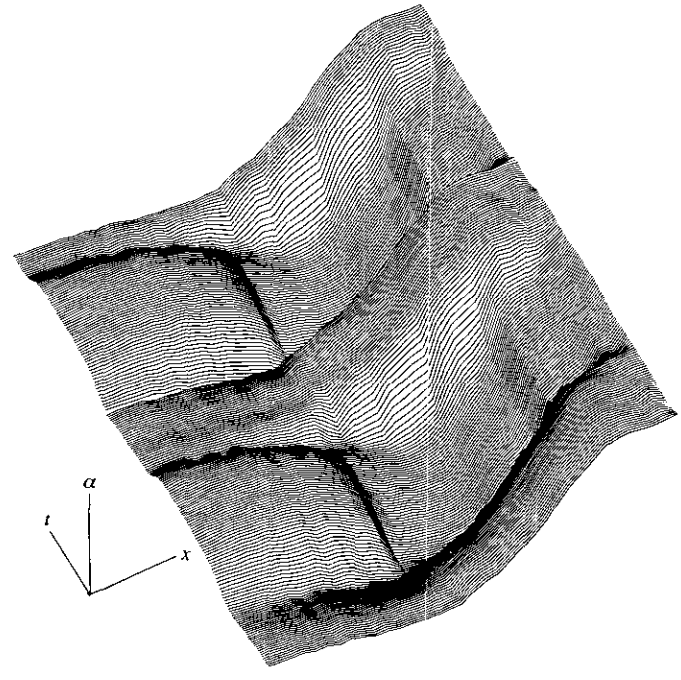

Figure 4. Area versus position and time. Lines show tube area versus x at fixed times. Parameter values: $p_u = 66$ and $\bar{p}_{e2} = 54{\cdot}5$ kPa, giving $\bar{Q} = 197$ ml/s. Frequency of oscillation: 4·6 Hz. Time increases away from the viewer. The 35 successive incremental recordings combined here show the downstream 15% of the tube.

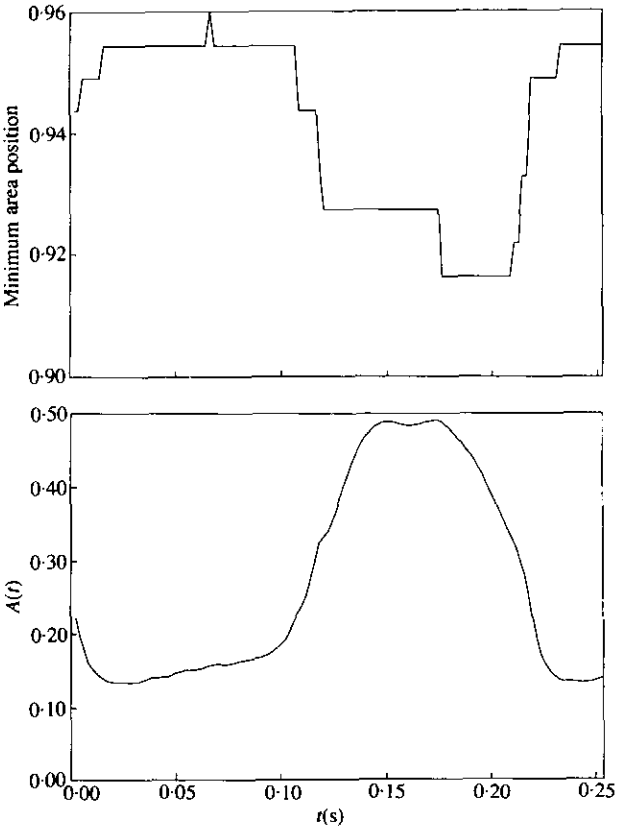

Figure 5. The position of the area minimum versus time, for the data shown in Figure 4. For phase reference, the waveform of minimum area versus time is also shown.

of the throat is in anti-phase with that downstream of the throat, in line with the predictions of the model (see Section 5).

The streamwise variation of the position of the point of minimum area during a cycle of the oscillation in Figure 4 is shown in Figure 5, along with a plot of the minimum throat area versus time, $A(t)$. Since the total range of the minimum area point spans only nine different catheter positions, corresponding to 10 mm, the position variation is somewhat crudely discretized. Nevertheless, the comparison shows clearly that the minimum moves downstream when it is small, and vice versa.

From the data in Figure 4 were also derived the profiles of area maximum and minimum versus position shown as dashed lines in Figure 6, and these in turn gave the area-oscillation amplitude profile shown as a solid line. The secondary maximum on the upstream shoulder of the main peak of the amplitude profile is now defined by several successive measurements and is clearly a real feature. On the other hand, the slight concavity of the main peak in this example is not consistently found. Notice that the point of "minimum maximum" is slightly upstream of the point of "minimum minimum"; this unexpected finding was consistent in our observations and was subsequently found to agree with the corresponding prediction. The apparent spatial maximum in the temporal area maximum very near the downstream end is a result of the finite wall thickness of the downstream pipe over which the tube was secured. This is because the impedance method can be thought of as measuring the crowding of

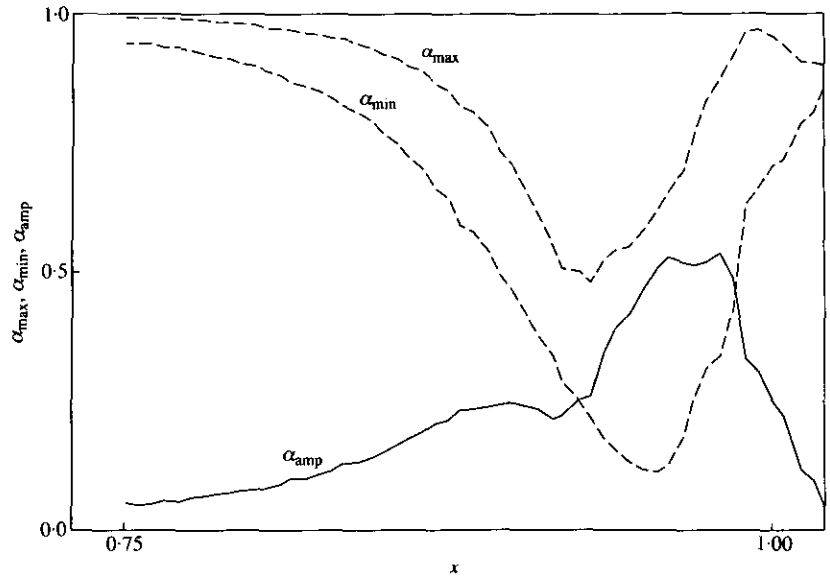

Figure 6. The envelope of the area oscillation shown in Figure 4 is given via dashed curves following the local area maximum and area minimum along the tube. Also shown (as a solid line) is the curve of local amplitude (cf. Figure 11).

current flux lines. The lines 'anticipate' the cross-sectional area change where the pipe lumen becomes the tube lumen. Furthermore, the electrodes measuring the local field gradient have, of necessity, finite length (2 mm) and spacing (1·6 mm). Thus, the recorded area does not indicate as sharply as might be expected the location of the end of the tube. The recording extends just into the pipe, so the maximum just outside is real, a consequence of the slight area step at the pipe entrance.

Finally, Figure 7 shows data for area versus position versus time for an *intermediate*-frequency (12 Hz) oscillation. When these are reduced to area-oscillation amplitude versus position as in Figure 8, the *same* pattern as for the low-frequency oscillation is seen; there is no evidence of a three-humped distribution as in Figure 12 below. This resemblance between I and L oscillations supports the view that they are both driven by essentially the same mechanism. Large-amplitude oscillations of these two modes cannot be readily differentiated *via* the area–distance profiles, however, contrary to the predictions of (small-amplitude) linear stability theory (Jensen & Pedley 1990b).

5. THEORETICAL PREDICTIONS

Figure 9 shows a numerical prediction of an LD oscillation. There are noticeable similarities between the waveform of this example and that shown in Figure 2, or in LD oscillation reported elsewhere, such as that in figure 6(b) of Bertram *et al.* (1990). On Figures 9 and 2 the oscillation has been broken down into six stages to help identify the common features. Both the minimum area, A, and the downstream pressure, p_2, fall sharply during (i), rise steeply during (ii) and less steadily during (iii); p_2 and A may then fall slightly [figure 6(b), Bertram *et al.* (1990)] before they resume a sharp rise during (iv) to their maxima. During (v) p_2 and A diminish slightly, and then finally in (vi) the collapse begins again. While the oscillation in Figure 2 tends to jump quite abruptly between two states, that in Figure 9 varies more smoothly. The resistance and inertia of the upstream and downstream rigid tubes account for the smooth variation of the flow rates Q_1 and Q_2 in Figure 9 relative to the corresponding pressures p_1 and p_2.

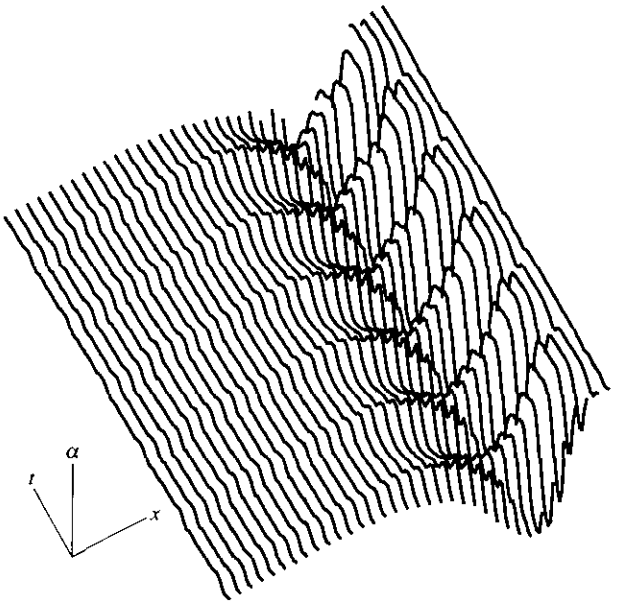

Figure 7. Area versus position and time, for an oscillation of intermediate frequency (12 Hz). Parameter values: p_u = 100 and $\bar{p}_{e2}$ = 51 kPa. Time increases away from the viewer. The 35 successive recordings shown here span the downstream 90 mm (39%) of the tube.

Comparison with the experimental results shown in Figures 1 and 4 can be made from Figure 10, in which the tube area for the oscillation shown in Figure 9 is plotted as a function of x and t over two periods. Notice that while the tube upstream and downstream of the throat appears to oscillate in fairly close antiphase in Figures 1 and 4, the relationship is less precise in Figure 10, where also the oscillation continues to have significant amplitude as far as the upstream end of the tube. Figure 11 shows the envelopes of the computed area oscillation and the distribution of area-oscillation amplitude along the length of the tube. (The curves in this figure are slightly irregular because the oscillation was sampled only 20 times during the cycle.) It is important to

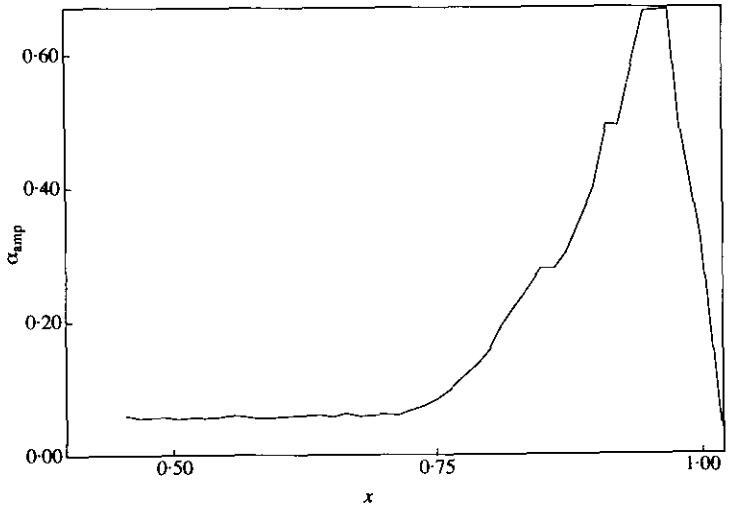

Figure 8. Area amplitude versus position for the same oscillation as in Figure 7, using all 47 recordings.

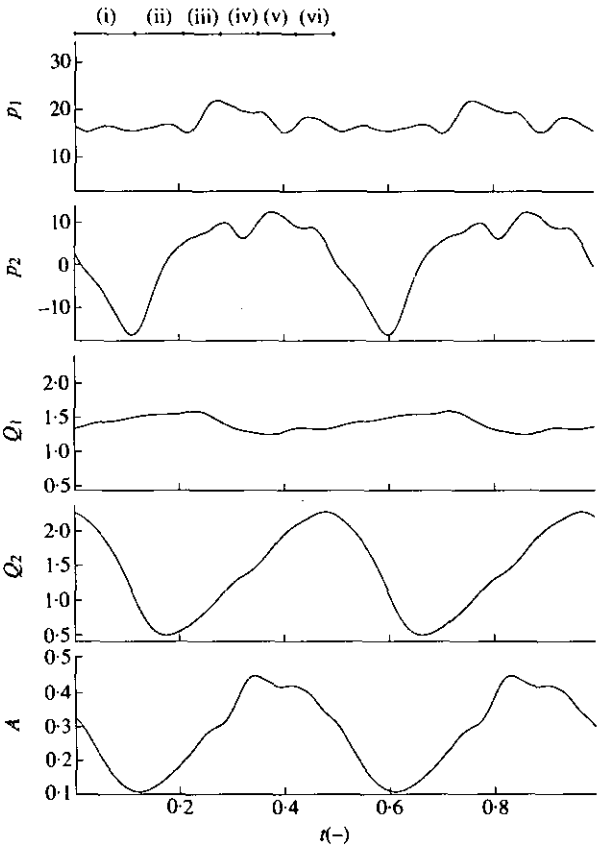

Figure 9. The nondimensional upstream and downstream pressures p_1, p_2, flow rate Q_1, Q_2 and minimum area A are plotted versus dimensionless time for a periodic low frequency oscillation. The oscillation is divided into six stages as indicated. The parameter values used for this oscillation were $P \equiv \hat{p}_e - p_2 = 15$, $Q = 1{\cdot}3$, so that $\hat{p}_u = 20{\cdot}44$, $\hat{p}_c = 16{\cdot}69$.

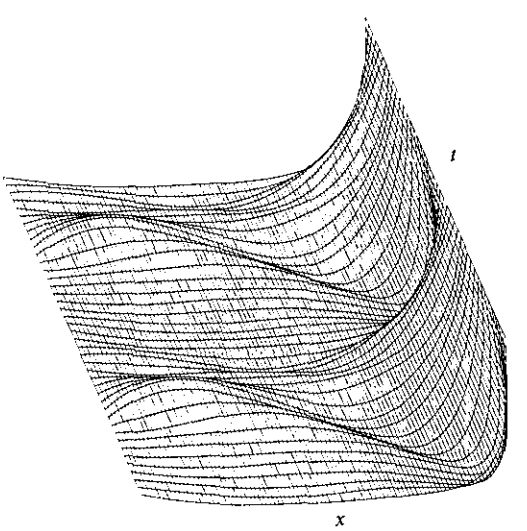

Figure 10. Tube area α is plotted versus x and t for the oscillation shown in Figure 9.

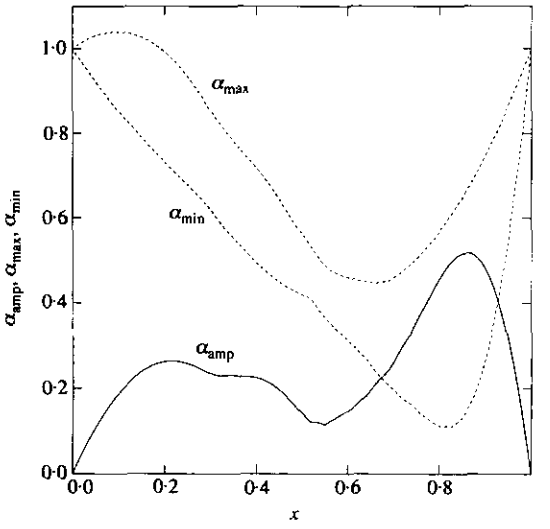

Figure 11. Area maximum and minimum and area amplitude, plotted versus x for the oscillation shown in Figure 9. The nondimensional tube length was chosen to be unity in these calculations. Compare with Figure 3.

note here a difference between theory (Figure 11) and experiment (e.g. Figure 6) in the proportion of the tube occupied by the throat; this is due in large part to differences in parameters. Computations of steady flows by Jensen & Pedley (1989) demonstrated that the throat/tube-length ratio was strongly dependent on Q, p_{e2}, and on the parameter $\lambda = L/L_0$, where L is the tube length and L_0 the length-scale of tube-deformation due to transverse bending and longitudinal tension: $\lambda = 1$ in the theory, and $\lambda = 25$ in the experiment. These fundamental differences must be borne in mind in what follows.

The greatest activity of both the experimental (Figure 3) and theoretical (Figure 11) oscillations was confined largely to the downstream end of the tube, and both amplitude distributions displayed two maxima. The upstream maximum of the theoretical oscillation extended to the upstream end of the tube, in line with the predictions of linear stability theory, but unlike those in Figure 3. The envelopes of the varying area distribution of the computed solution and the observations share the feature that the "minimum maximum" is upstream of the "minimum minimum". The area envelope of an intermediate-frequency oscillation [the "mode 3" oscillation shown in figures 4 and 5 of Jensen (1992)] is shown in Figure 12. As in Figure 11, the small irregularities in the curves in Figure 12 are associated with discrete temporal sampling. Three maxima are evident, the largest and most distinct very close to the downstream end of the tube ($0{\cdot}75 < x < 1$), and two lower ones at $0 < x < 0{\cdot}3$ and $0{\cdot}3 < x < 0{\cdot}75$. Recall that a three-humped shape was not observed experimentally (Figure 8). Again, the difference in the degree of activity at the upstream end of the tube between Figures 8 and 12 suggests a considerable discrepancy in parameters, or an inherent inadequacy in the model.

6. EVENTS DURING A CYCLE

To understand more of what is going on in the example of Figure 9 it is helpful to look at the complete area, flow speed, and pressure distributions of the oscillation. These are shown in Figure 13(i)–(vi), with each stage corresponding to those shown in

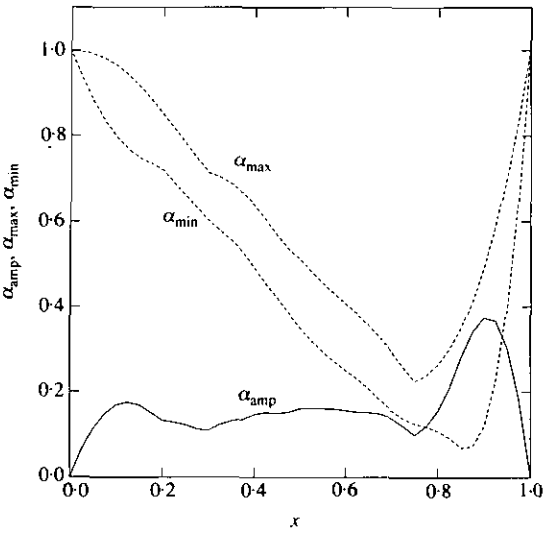

Figure 12. Area maximum/minimum and amplitude plotted versus x for the intermediate frequency oscillation shown in figures 4 and 5 of Jensen (1992).

Figure 9. Six separate panels were necessary, as three-dimensional views of the four variables were not sufficiently clear. α, u, p and the dissipation d (see Section 3) were calculated at 20 intervals throughout the cycle, and are plotted in Figure 13 over consecutive intervals as functions of x throughout the six stages. The paths traced out during each stage of the cycle by the points of minimum area and maximum flow speed are indicated by solid lines in the two upper right-hand panels.

The details of the oscillation are described in detail stage-by-stage below, referring primarily to Figure 13. Comments related to experimental data are enclosed in square brackets.

(i) Initially the tube undergoes sudden collapse at its downstream end. The phase begins with a moderate constriction near $x = 0{\cdot}7$. With a high flow speed here, and quite substantial retardation beyond, d is sizeable enough for there to be little pressure recovery across the region of separated flow. p_2 is indeed sufficiently low to encourage further collapse, and so the constriction narrows further and moves downstream, and the maximum speed increases rapidly, although the point of maximum speed (the separation point) remains almost stationary. With growing velocity gradients, d increases rapidly, but remains confined to a very narrow zone. This enhances the drop in the downstream pressure, and the collapse proceeds almost unrestrained. [The observed oscillations had a more rapid closure phase than is indicated by the theory here (compare Figures 2 and 9).]

(ii) Ultimately, however, the high longitudinal tensile forces and the increasing transverse bending stresses in the tube wall at the constriction are sufficiently large to oppose further reductions in area. In addition, the tube wall upstream of the constriction acts as a partial barrier to fluid entering the tube, and so the force arising from the pressure of the fluid on the wall has a large longitudinal component. The combination of elastic and inertial forces makes the tube bulge slightly upstream of the constriction, obliging the constriction to widen and move upstream. Accordingly, the maximum speed decreases, the separation point moves upstream, velocity gradients lessen and d falls in magnitude, allowing greater pressure recovery where the flow is

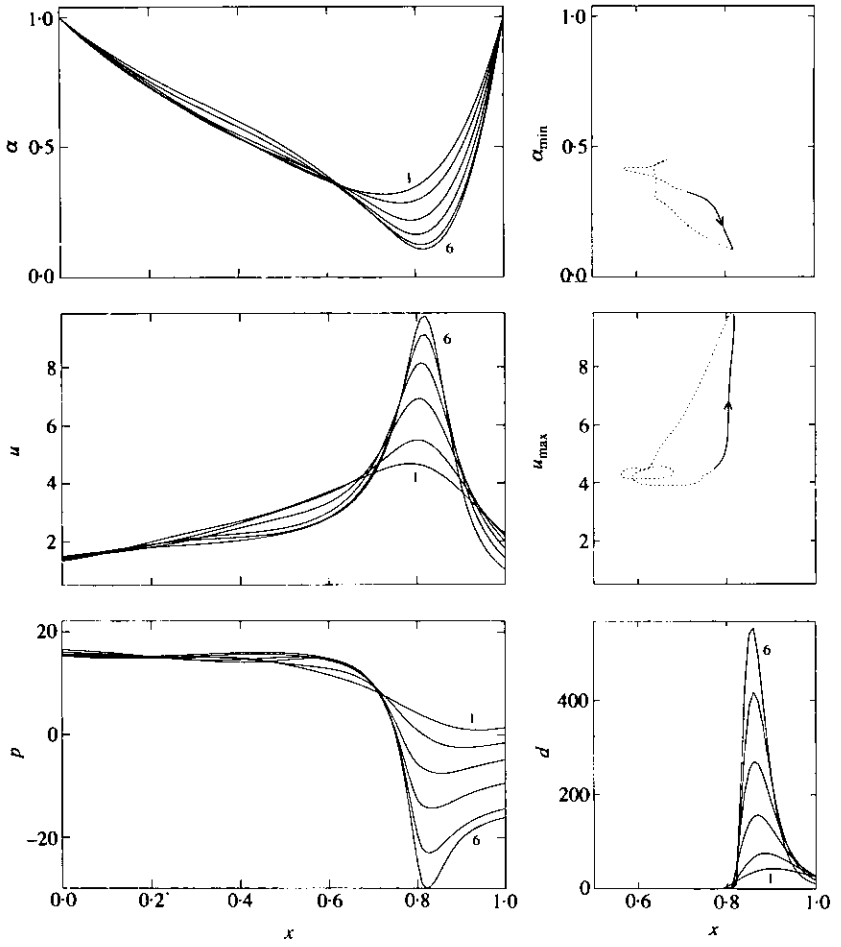

Figure 13(i). The oscillation shown in Figures 9 and 10 is shown in more detail in figures (i)–(vi), each of which contains six panels. The left-hand column and bottom right-hand panel in each figure show the area, α, velocity, u, pressure, p and dissipation, d, as functions of x and t at evenly spaced intervals during stages (i)–(vi), as shown in Figure 9. The two upper right-hand panels show the paths of the point of minimum area, α_{min}, and the point of maximum velocity (the separation point) u_{max}; the segments of each path corresponding to each stage of the oscillation are plotted as solid lines; dotted lines show their complete paths. The direction of increasing time is shown by arrows on the paths of α_{min} and u_{max}, and by numbers labelling the curves in the remaining panels.

separated, and so p_2 rises rapidly. [Figure 5 above, which showed the measured motion of the minimum area versus time, demonstrates that the predicted path of α_{min} is realistic.]

(iii) As the constriction continues to widen, the bulge due to the inertia of the fluid entering the tube moves further upstream. (This upstream propagation demonstrates the dispersive effect of longitudinal tension: the speed c of long-wavelength waves along the upstream third of the tube, where $0{\cdot}8 < \alpha < 1{\cdot}0$, varies between 1·2 and 1·5, precisely the range of flow speeds, u, in this region; it is because it has a sufficiently short wavelength that this bulge can propagate against the flow.) As it enters regions of increasing α, i.e. regions of increasing compliance, the bulge increases in amplitude so that the tube distends suddenly at its upstream end; correspondingly p_1 rises very steeply. Ultimately longitudinal tension restrains the distension of the tube. [Note that

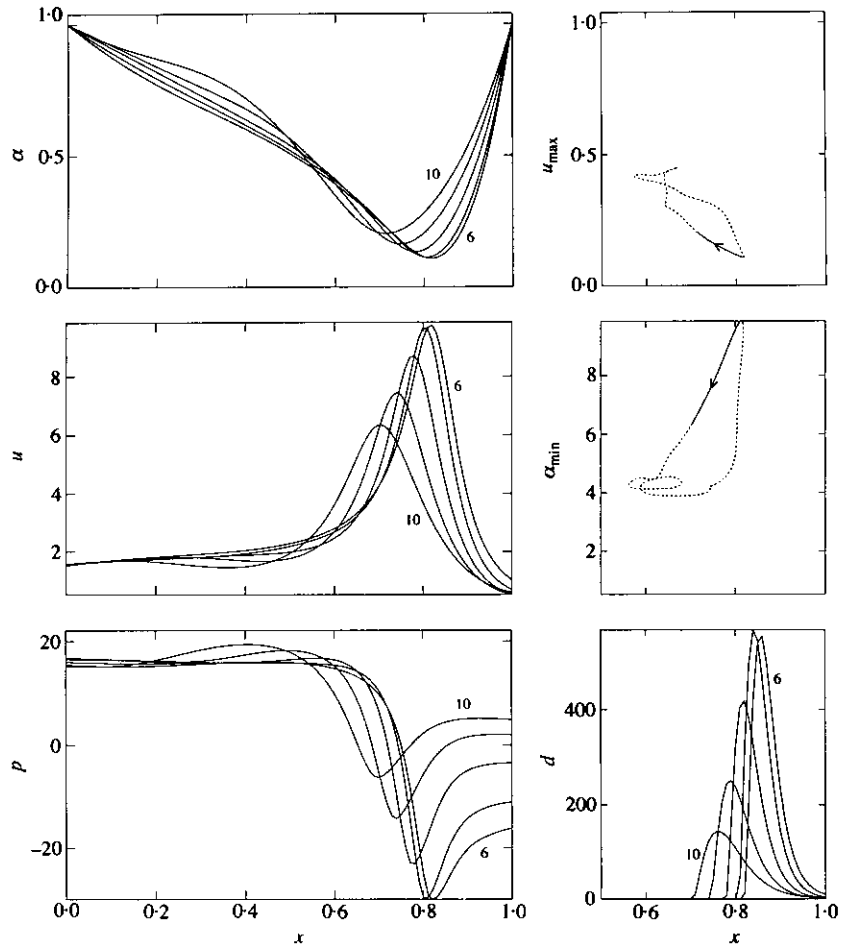

Figure 13(ii)

although p_1 rises very steeply during this phase in Figure 9, such large changes in area at the upstream end of the tube, in particular those giving rise to $\alpha > 1$, are not observed experimentally. Again, this is partly due to differences in parameters, and partly because such behaviour is less likely to be exhibited by a thick-walled tube. The bulge directly upstream of the throat in Figures 1, 3, 4 and 6(b) appears never to travel all the way upstream. This may be because the throat/tube-length ratio in the experiments is much smaller than that in the calculations, making the theoretical results more strongly influenced by the upstream boundary conditions. Further experiments are needed to test whether upstream conditions become less important as the tube length increases.]

(iv) This phase begins with the tube distended over $0 < x < 0{\cdot}2$, and having a steep area gradient over $0{\cdot}2 < x < 0{\cdot}6$, so that, as in (ii), inertial forces open the constriction further. However, with the sudden bulging of the tube at its upstream end comes an abrupt change in the direction of the path of the point of minimum area, which no longer moves upstream but remains approximately stationary. Meanwhile the velocity distribution flattens, and its maximum moves rapidly up and downstream. Thus the length of the zone of dissipation varies considerably, although the amount of energy loss is relatively small. [The re-opening in the experiment is more rapid than in the model. The rather complex activity in the motion of the separation point may be an

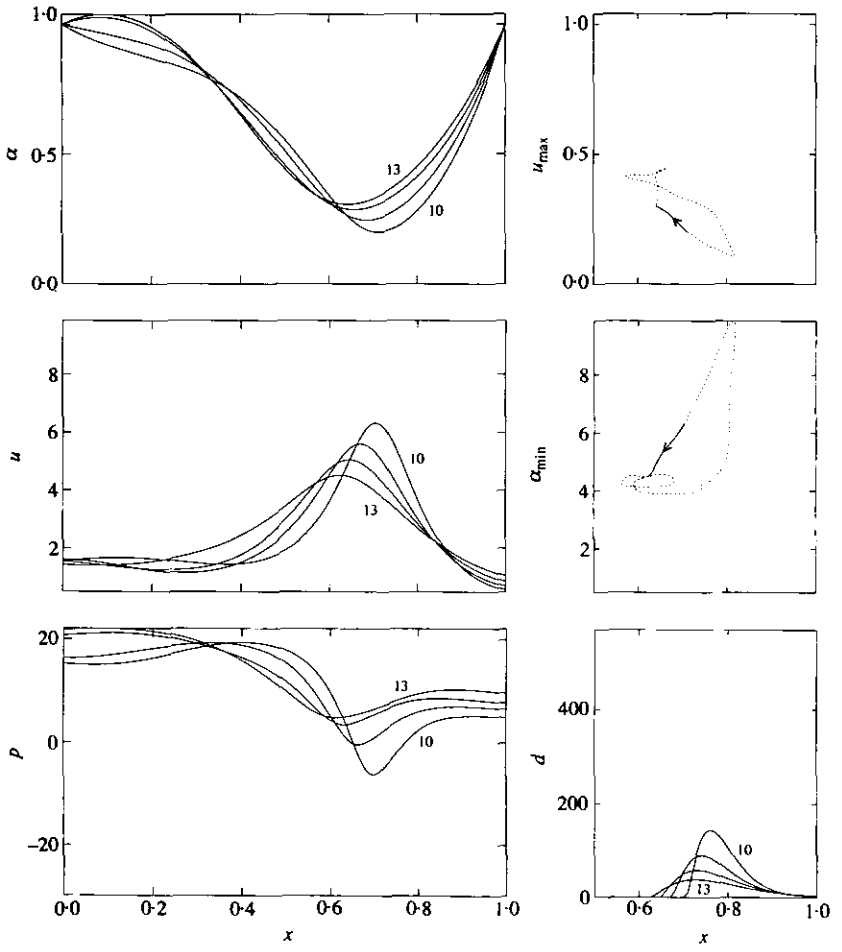

Figure 13(iii)

artefact of the model. Flow visualization could in principle check this, albeit with great difficulty in this time-varying turbulent flow.]

(v) Throughout this stage the tube remains in a mildly collapsed state, with the area profile relatively flat. The dissipation is therefore very weak. There is considerable activity in p_1 and p_2 (see Figure 9), apparently the remnants of the disturbances generated during stages (i)–(iii). Although it is difficult to identify waves and their reflections from Figure 13, the time series on Figure 9 suggest that the sudden large rise in p_1 during (iii) results in a similar, but smaller rise in p_2 during (iv), and a further, even smaller rise in p_1 during (v). (Each of these three events is separated by about 0·1 units of time, implying that the average wave speed is near 10; to check that this speed was not unreasonably large, the speed at which short waves generated by a sudden perturbation travel the length of the tube was estimated numerically for these parameter values, and found to be as great as 20.) [If similar area variations due to upstream and downstream wave propagation do occur experimentally, they are so weak as to be lost in measurement noise. In principle, subnoise-level waves could be revealed by ensemble-averaging many cycles. However, the experimental finding that frequency of oscillation is not governed by tube length (Bertram *et al.* 1990) seems to indicate that end-to-end wave propagation is not a significant factor in the observed oscillations.]

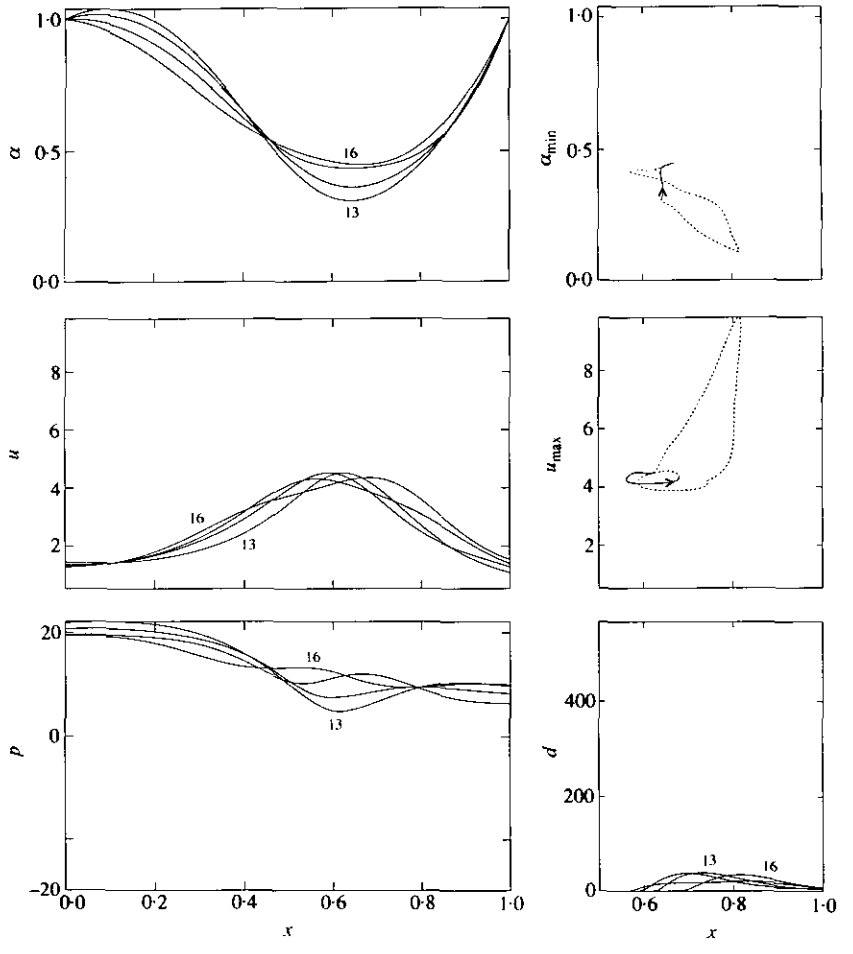

Figure 13(iv)

(vi) During this final stage, the point of maximum flow speed moves downstream very rapidly. This also occurred in stage (iv), but then p_2 and α_{min} were both increasing—in this case p_2 is roughly constant and the tube area is decreasing. In these conditions the tube can continue collapsing (leading to the events of stage (i)), and this is enhanced by the fact that u_{max} comes closer to the downstream end of the tube, so that velocity gradients (and dissipation) are larger.

While Figure 13 shows very little activity during stages (ii) and (iii) and stages (v) and (vi) (so that the tube appears to jump abruptly between two almost static states), the numerical results suggest that the remnants of pressure disturbances propagating up and down the tube affect the position of the separation point and the point of minimum area during these phases. This activity might lead to the abrupt transitions during (i) and (iv).

7. DISCUSSION

In view of the difficulties of quantitative comparison of the model with experiment, it is pertinent to examine the development of both the assumptions underlying the model

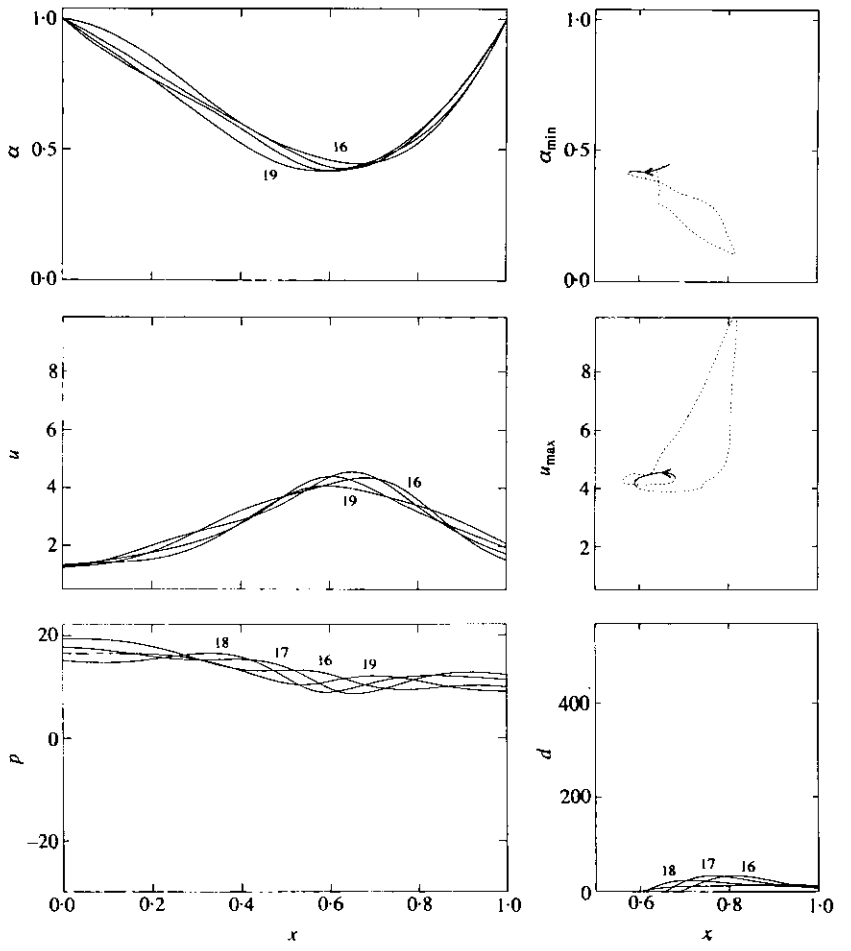

Figure 13(v)

and the choice of experimental parameters, and the reasons for their adoption in each case.

The experiments form part of a continuous programme in which the collapsible tubes first reported on by Bertram (1986) have been progressively investigated in different ways. The programme was designed to address a situation where theoretical modelling was limited by the large variety of incompletely reported experiments in the literature. In a series of papers, a more comprehensive picture has been built of the behaviour of a particular type of collapsible tube than has ever been assembled before. A deliberate choice was made to examine the behaviour of relatively thick-walled collapsible tubes. These represented a relatively neglected area, in that previous experiments had concentrated on tubes of either moderate or very small circumferential bending stiffness, despite the fact that theory emphasized the local tube law as a source of elastic restoring force. They offered the advantage that nowhere in a large region of operating-point space did self-excited oscillation involve the tube being sucked into the downstream rigid mounting pipe. The gross sudden change in wall properties between a very compliant thin-walled tube and a rigid pipe is unphysiological (Kamm 1987), although effects manifested only by such configurations can still be of considerable interest. The extreme instantaneous tube shapes involved are also not readily

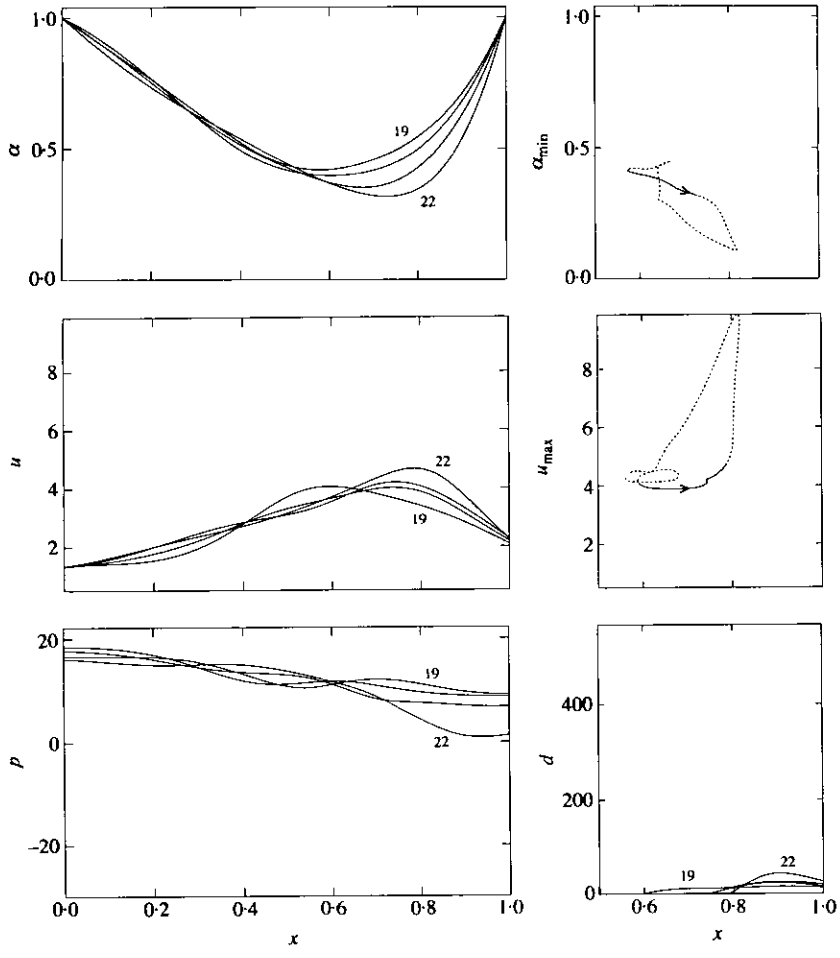

Figure 13(vi)

modelled. Bertram *et al.* (1989) have since shown that effects arising from such a discontinuity do not dominate the behavour of the thicker-walled tubes dealt with here.

The one-dimensional model, on the other hand, is based upon a long-wavelength assumption ($L_0 \gg D_0$, see Section 3) that is not satisfied by the thick-walled tubes used in the experiments because of their large bending stiffnesses. The model, known to be quantitatively accurate for steady flows in thin-walled tubes, is therefore at best qualitatively accurate in the present case. This discourages efforts to improve the quantitative fit of the model to the experiments by varying other parameters in the system. For instance, the conduits up- and downstream of the collapsible tube were assumed by Jensen (1990a) to contribute unit dimensionless resistance to flow and fluid inertance, whereas the corresponding experimental parameters relating pressure drop to flow-rate squared and to rate of flow-rate change, respectively, were in the range 5–10 for resistance and 500 for inertance (see Appendix A). The frequency of self-excited oscillation is a powerful function of the up- and downstream inertance, as is shown for a limited range in Figure 14. This result is taken from the lumped-parameter model of Bertram & Pedley (1982), but is expected to be as true for the hybrid model here as it is experimentally. (In passing, we note that this means that the large quantitative disparity in predicted frequency of oscillation between lumped-parameter

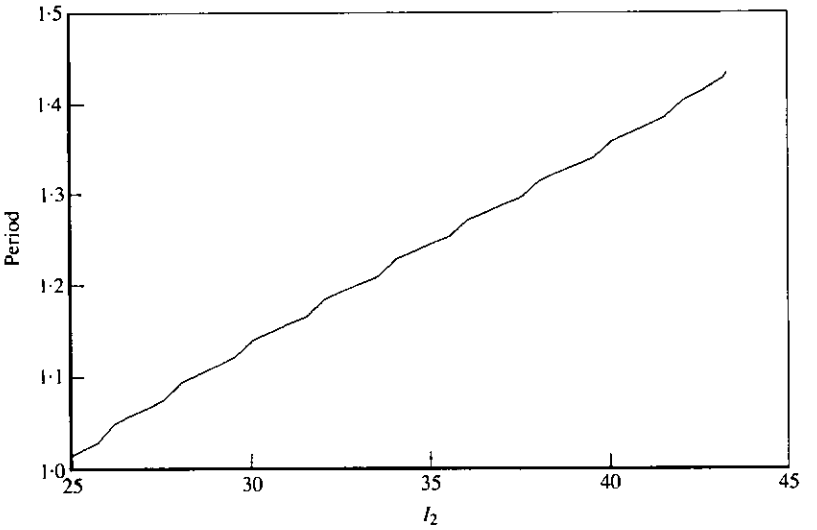

Figure 14. Variation of period of oscillation with up- and downstream fluid inertia, as predicted by the lumped-parameter model of Bertram & Pedley (1982). In their notation, the dimensionless model parameters were $P_{11}(\equiv p_u) = 150$, $P_e = 200$, $P_k = 4$, $R_k = 0{\cdot}00466$, $l = 10$, $R_2 = 75$, and $r = R_1/R_2 = I_1/I_2 = 0{\cdot}5$.

and one-dimensional models noted by Bertram *et al.* (1989) cannot necessarily be used to infer which is a better model of the prevailing oscillation mechanism in a given experiment.) Despite the anticipated improvement in predicted frequency fit to the experimental results, we have not therefore considered it worthwhile to compute numerical results with these parameters quantitatively matched to the experimental values while more fundamental discrepancies necessarily go uncorrected.

In summary, a new technique involving conductimetric catheterization at a sequence of axial locations has been used to measure the area-distance profile of some strictly periodic, low-frequency (LD) oscillations of a collapsed tube. In the cases examined, significant fluctuations in the cross-sectional area were shown to be confined to roughly the downstream third of the tube; in this region the area-oscillation amplitude had a large but narrow peak, with a smaller local maximum on its upstream shoulder. These results were compared with numerical predictions of a one-dimensional model, the central feature of which was a simple approximation of the dissipation associated with flow separation; the model had previously been shown to describe many significant features of collapsible-tube flows, although precise quantitative comparison with these experiments was not possible. Although the area–distance profiles of a nonlinear LD oscillation predicted by the model also had two peaks, they were spread further apart and there was a more uniform distribution of area fluctuations along the length of the tube; this difference can be accounted for to some extent by discrepancies in parameters used in theory and experiment. However, the computations captured many of the other observed features of LD oscillations, evident particularly in the pressure measurements at each end of the tube.

Because of the success of the model in describing some of the more robust features of the LD oscillation measured here, and of those measured previously (Bertram *et al.* 1990), the experimental and model results were then used together to examine the mechanism of the oscillation. The advantage of having both sets of results available was that the model gave a reasonably reliable indication of the behaviour of internal fluid-dynamical parameters (such as the position of the separation point) that are currently difficult either to visualize or to measure. The oscillation was broken down into

six distinct stages, during which the tube collapses violently at its downstream end [(i)–(iii) in Figures 9 and 13] and then during which it is less severely constricted and the remnants of pressure disturbances propagate up- and downstream, (iv)–(vi). The collapse is driven by the fall in downstream pressure resulting from the strong dissipation in the separated-flow region beyond the throat of the tube, but opposed by elastic forces and by the compliance of the section of the tube upstream of the throat.

Thus, the experimental and numerical results together demonstrate that the energy loss associated with flow separation is a significant factor in driving the LD class of self-excited oscillation. Because intermediate-frequency (I) oscillations exhibited many qualitative features (both experimentally and theoretically) that strongly resembled the LD results, it is likely that these classes of oscillation share a common mechanism. The other class of low-frequency oscillations (LU), however, could not be modelled successfully, suggesting either that additional sophistication in modelling the motion of the separation process is required (perhaps by incorporating hysteresis in the motion of the separation point), or that additional effects, perhaps beyond the scope of a one-dimensional description, are at work. Further experimental measurements of variables taken along the length of the tube, particularly relating to the internal fluid dynamics, will be an essential part of this investigation.

ACKNOWLEDGEMENTS

The experiments were funded by the Australian Research Council. O. E. Jensen was supported by a U.K. SERC Research Studentship and a bursary from Smith Associates Ltd. We thank J. P. Armitstead for computing the results shown in Figure 14.

REFERENCES

BERTRAM, C. D. 1986 Unstable equilibrium behaviour in collapsible tubes. *Journal of Biomechanics* **19,** 61–69.

BERTRAM, C. D. 1987 The effects of wall thickness, axial strain and end proximity on the pressure-area relation of collapsible tubes. *Journal of Biomechanics* **20,** 863–876.

BERTRAM, C. D. & PEDLEY, T. J. 1982 A mathematical model of unsteady collapsible tube behaviour. *Journal of Biomechanics* **15,** 39–50.

BERTRAM, C. D., RAYMOND, C. J. & BUTCHER, K. S. A. 1989 Oscillations in a collapsed-tube analog of the brachial artery under a sphygmomanometer cuff. *ASME Journal of Biomechanical Engineering* **111,** 185–181.

BERTRAM, C. D., RAYMOND, C. J. & PEDLEY, T. J. 1990 Mapping of instabilities for flow through collapsed tubes of differing length. *Journal of Fluids and Structures* **4,** 125–153.

BERTRAM, C. D., RAYMOND, C. J. & PEDLEY, T. J. 1991 Application of nonlinear dynamics concepts to the analysis of self-excited oscillations of a collapsible tube conveying a flow. *Journal of Fluids and Structures* **5,** 391–426.

BERTRAM, C. D. & RIBREAU, C. 1989 Cross-sectional area measurement in collapsed tubes using the transformer principle. *Medical and Biological Engineering and Computing* **27,** 357–364.

BERTRAM, C. D. & SHEPPEARD, M. D. 1991 Internal cross-sectional area versus axial position and time for collapsible tubes undergoing self-excited oscillation. *Medical and Biological Engineering and Computing* **29,** Supplement Part 1, 258.

BONIS 1979 Ecoulement visqueux permanent dans un tube collabable elliptique. Thèse de Doctorat d'Etat, Université de Technologie de Compiègne, France.

CANCELLI, C. & CHIOCCHIA, G. 1979 On the onset of self-excited oscillations in a collapsible tube flow with sonic index values less than one: mathematical model and numerical results. *Atti della Accademia Nazionale dei Lincei—Memorie Serie VIII (Classe di Scienze fisiche, matematiche e naturali)* **15,** 319–352.

CANCELLI, C. & PEDLEY, T. J. 1985 A separated-flow model for collapsible tube oscillations. *Journal of Fluid Mechanics* **157,** 375–404.

CONRAD, W. A. 1969 Pressure-flow relationships in collapsible tubes. *IEEE Transactions on Biomedical Engineering* **16,** 284–295.

ELAD, D., SAHAR, M., AVIDOR, J. M. & EINAV, S. 1992 Steady flow through collapsible tubes: measurements of flow and geometry. *ASME Journal of Biomechanical Engineering* **114,** 84–91.

JENSEN, O. E. 1990a Flow in collapsible tubes. Ph.D. thesis, University of Cambridge, U.K.

Jensen, O. E. 1990b Instabilities of flow in a collapsed tube. *Journal of Fluid Mechanics* **220,** 623–672.

JENSEN, O. E. 1992 Chaotic oscillations in a simple collapsible tube model. *ASME Journal of Biomechanical Engineering* **114,** 55–59.

JENSEN, O. E. & PEDLEY, T. J. 1989 The existence of steady flow in a collapsed tube. *Journal of Fluid Mechanics* **206,** 339–374.

KAMM, R. D. 1987 Flow through collapsible tubes. In *Handbook of Bioengineering* (eds R. Skalak & S. Chien), Chapter 23. New York: McGraw-Hill.

KECECIOGLU, I., MCCLURKEN, M. E., KAMM, R. D. & SHAPIRO, A. H. 1981 Steady, super-critical flow in collapsible tubes. Part 1. Experimental observations. *Journal of Fluid Mechanics* **109,** 367–389.

LYON, C. K., SCOTT, J. B., ANDERSON, D. K. & WANG, C. Y. 1981 Flow through collapsible tubes at high Reynolds numbers. *Circulation Research* **49,** 988–996.

MATSUZAKI, Y. & MATSUMOTO, T. 1989 Flow in a two-dimensional collapsible channel with rigid inlet and outlet. *ASME Journal of Biomechanical Engineering* **111,** 180–184.

MAZGHI, M. 1986 Ecoulement visqueux permanent dans un tube collabable incliné: étude expérimentale. Thèse de 3ème cycle, Université Paris XII, France.

MCCLURKEN, M. E. 1978 Shape-independent area measurement in collapsible tubes by an electrical impedance technique. *Proceedings of the 31st Annual Conference on Engineering in Medicine and Biology,* Atlanta GA, p. 95.

MCCLURKEN, M. E., KECECIOGLU, I., KAMM, R. D. & SHAPIRO, A. H. 1981 Steady, super-critical flow in collapsible tubes. Part 2. Theoretical studies. *Journal of Fluid Mechanics* **109,** 391–415.

OHBA, K., YONEYAMA, N., SHIMANAKA, Y. & MAEDA, H. 1984 Self-excited oscillation of flow in collapsible tube. Technical Reports of Kansai University, no. 25, Japan.

ROACHE, P. J. 1976 *Computational Fluid Dynamics.* Hermosa Publ.

ROSENBERG, N., ZELTSER, R., ELAD, D., SAHAR, M., AVIDOR, J. M. & EINAV, S. 1990 Simplified remote sensing of three-dimensional surfaces: application for biomedical engineering. *Photogrammetric Engineering and Remote Sensing* **56,** 1273–1280.

SCHOENDORFER, D. W. & SHAPIRO, A. H. 1977 The collapsible-tube as a prosthetic vocal source. *Proceedings of the San Diego Medical Symposium* **16,** 349–356.

APPENDIX A: THE THEORETICAL MODEL: SCALINGS AND PARAMETERS

The scalings and parameters used in the model are presented here. For further details, see Cancelli & Pedley (1985), Jensen & Pedley (1989), Jensen (1990a,b) and Jensen (1992). We define the following variables, using tildes to denote that they are dimensional: the distance along the tube from its upstream end, $\tilde{x}$; time, $\tilde{t}$; the tube cross-sectional area, $\tilde{\alpha}(\tilde{x}, \tilde{t})$; the cross-sectionally averaged flow speed, $\tilde{u}(\tilde{x}, \tilde{t})$; the cross-sectionally averaged internal pressure, $\tilde{p}(\tilde{x}, \tilde{t})$. The relevant parameters are as follows, with the experimental values of each given in parentheses: the fluid density, ρ (10^3 kg m^{-3}); the tube length, L (0·235 m); the pressure external to the tube, p_e; the tube circumferential bending stiffness, K_p (11·4 kPa); the tube cross-sectional area and diameter when unstressed, α_0 and d_0 (13·5 mm internally); the longitudinal tension per unit perimeter, T (74 N m^{-1}); the upstream head, p_u; and the resistances k_i and inertances l_i of the rigid segments upstream ($i = 1$) and downstream ($i = 2$) of the collapsible tube ($k_1 = 2{\cdot}4 \times 10^{11}$ kg m^{-7}, $k_2 = 5{\cdot}4 \times 10^{11}$ kg m^{-7}, $l_1 = 3{\cdot}8 \times 10^7$ kg m^{-4}, $l_2 = 3{\cdot}3 \times 10^7$ kg m^{-4}).

Defining a velocity-scale $c_0 = (K_p/\rho)^{1/2}$, and a length-scale, $L_0 = (D_0 T/K_p)^{1/2}$, we then use the following nondimensionalization scheme: $\tilde{x} = L_0 x$; $\tilde{t} = (L_0/c_0)t$; $\tilde{\alpha}(\tilde{x}, \tilde{t}) = \alpha_0 \alpha(x, t)$; $\tilde{u}(\tilde{x}, \tilde{t}) = c_0 u(x, t)$; $\tilde{p}(\tilde{x}, \tilde{t}) = K_p p(x, t)$; $p_e = K_p \hat{p}_e$; $p_u = K_p \hat{p}_u$; $L = L_0 \lambda$; $k_{1,2} = (\rho/\alpha_0^2)\eta_{1,2}$; $l_{1,2} = (\rho L_0/\alpha_0)\lambda_{1,2}$.

The boundary conditions corresponding to the governing equations given in Section 3 are

$$\alpha(0, t) = \alpha(\lambda, t) = 1,$$
$$p(0, t) = \hat{p}_u - (\tfrac{1}{2} + \eta_1)u^2(0, t) - \lambda_1 u_t(0, t),$$
$$p(\lambda, t) = \eta_2 u^2(\lambda, t) + \lambda_2 u_t(\lambda, t).$$

The nondimensional parameters were not chosen to match the experiment directly, but as follows: $k = 45$, $\lambda = 1$, $\eta_1 = \eta_2 = 1$ and $\lambda_1 = \lambda_2 = 1$. Note that by using experimental parameter values, the length-scale $L_0 = 9{\cdot}4$ mm, and the velocity-scale $c_0 = 3{\cdot}38\ \mathrm{m\,s^{-1}}$, so the timescale $L_0/c_0 = 2{\cdot}8 \times 10^{-3}$ s, two orders of magnitude smaller than the timescale of the oscillations, indicating that the scaling of the model under assumptions (i–iv) (see Section 3) is not directly appropriate for the experiment. Corresponding values of the nondimensional groups for the experiment were $k = 67$; $\lambda = 25$, $\eta_1 = 4{\cdot}9$, $\eta_2 = 11$, $\lambda_1 = 578$ and $\lambda_2 = 502$.

APPENDIX B: LONGITUDINAL BENDING STIFFNESS

Suppose that assumptions (ii) and (iii) in Section 3 hold. Using the pressure–area relation of McClurken *et al.* (1981), we can estimate the strength of the three dominant contributions to the transmural pressure: circumferential bending stiffness generates pressures of $\mathcal{O}(K_p)$; the total longitudinal tension T_l ($= \pi D_0 T$) generates pressures of $\mathcal{O}(T_l/X^2)$, where X is the length-scale over which the tube is deformed; and longitudinal bending stiffness B [$= K_p D^4/8$; McClurken *et al.* (1981)] generates pressures of $\mathcal{O}(B/X^4)$. There are, therefore, three distinct length-scales over which pairs of these forces are of the same order of magnitude: $X_{TK} = (T_l/K_p)^{1/2}$, $X_{BT} = (B/T_l)^{1/2}$ and $X_{BK} = (B/K_p)^{1/4}$. Note that $X_{BK}^2 = X_{BT}X_{TK}$. The relative sizes of the forces can be determined by considering the nondimensional parameter $M = BK_p/T_l^2 = (X_{BT}/X_{TK})^2$. Clearly if $M = \mathcal{O}(1)$, all three length-scales are of the same order, and the three effects will be of equal importance.

Suppose that the dominant balance is between circumferential and longitudinal bending. Then $X = X_{BK}$, and longitudinal tension is negligible provided $M \gg 1$. The case assumed by the theory under assumption (iv) is that longitudinal bending is negligible compared to the remaining two forces. In this case $X = X_{TK}$ and $M \ll 1$. For there to be a dominant balance between longitudinal bending and longitudinal tension, we require $X = X_{BT}$ and $M \ll 1$ also. Thus, when $M \ll 1$, so that $X_{BT} \ll X_{TK}$, the dominant balance is between longitudinal tension and transverse bending over a length-scale X_{TK}; longitudinal bending may be important over a much smaller length-scale X_{BT}, in regions of rapid change (e.g., at the boundaries of the tube).

The value of M corresponding to the experimental parameter values is 0·4, indicating that all three forces are likely to be of the same order of magnitude in this case. The tube deformation can be expected to have a length-scale of the order of $L_0 \simeq 10$ mm (L_0 and X_{TK} differ only by a numerical factor; recall that in comparison the total tube length is 235 mm. Figure 1 confirms that the deformation length-scale is substantially shorter than the total length of the tube, as it is only the downstream 15% of the tube that is significantly collapsed.